Double-free-layer stochastic magnetic tunnel junctions with synthetic antiferromagnets

Kemal Selcuk,[1,*] Shun Kanai,[2,3,4,5,6,7,8] Rikuto Ota,[2,3] Hideo Ohno,[2,4,5,9] Shunsuke Fukami,[2,3,4,5,9,10] and Kerem Y. Camsari[1,†]

[1] *Department of Electrical and Computer Engineering, University of California, Santa Barbara, California 93106, USA*

[2] *Research Institute of Electrical Communication, Tohoku University, 2-1-1 Katahira, Aoba-ku, Sendai 980-8577, Japan*

[3] *Graduate School of Engineering, Tohoku University, 6-6 Aramaki Aza Aoba, Aoba-ku, Sendai 980-8579, Japan*

[4] *WPI Advanced Institute for Materials Research (WPI-AIMR), Tohoku University, 2-1-1 Katahira, Aoba-ku, Sendai 980-8577, Japan*

[5] *Center for Science and Innovation in Spintronics (CSIS), Tohoku University, 2-1-1 Katahira, Aoba-ku, Sendai 980-8577, Japan*

[6] *PRESTO, Japan Science and Technology Agency (JST), Kawaguchi 332-0012, Japan*

[7] *Division for the Establishment of Frontier Sciences of Organization for Advanced Studies at Tohoku University, Tohoku University, Sendai 980-8577, Japan*

[8] *National Institutes for Quantum Science and Technology, Takasaki 370-1207, Japan*

[9] *Center for Innovative Integrated Electronic Systems (CIES), Tohoku University, 468-1 Aramaki Aza Aoba, Aoba-ku, Sendai 980-0845, Japan*

[10] *Inamori Research Institute of Science (InaRIS), Kyoto 600-8411, Japan*

(Received 13 November 2023; revised 6 March 2024; accepted 29 March 2024; published 1 May 2024)

Stochastic magnetic tunnel junctions (SMTJs) using low-barrier nanomagnets have shown promise as fast, energy-efficient, and scalable building blocks for probabilistic computing. Despite recent experimental and theoretical progress, SMTJs exhibiting the ideal characteristics necessary for probabilistic bits (p-bits) are still lacking. Ideally, the SMTJs should have (a) voltage bias independence, preventing read disturbance; (b) uniform randomness in the magnetization angle between the two magnetic layers; and (c) fast fluctuations without requiring external magnetic fields, while being robust to magnetic field perturbations. Here, we propose a design that satisfies all of these requirements, using double-free-layer SMTJs with synthetic antiferromagnets (SAFs). We evaluate the proposed SMTJ design with experimentally benchmarked spin-circuit models, accounting for transport physics, coupled with the stochastic Landau-Lifshitz-Gilbert equation for magnetization dynamics. We find that the use of low-barrier SAF layers reduces dipolar coupling, achieving uncorrelated fluctuations at zero-magnetic field, surviving up to diameters exceeding $D \approx 100$ nm if the nanomagnets can be made thin enough ($\approx$ 1–2 nm). The double-free-layer structure retains bias independence and the circular nature of the nanomagnets provides near-uniform randomness with fast fluctuations. Combining our full SMTJ model with advanced transistor models, we estimate the energy to generate a random bit to be about 3.6 fJ, with fluctuation rates of about 3.3 GHz per p-bit. Our results will guide the experimental development of superior stochastic magnetic tunnel junctions for large-scale and energy-efficient probabilistic computation for problems relevant to machine learning and artificial intelligence.

DOI: 10.1103/PhysRevApplied.21.054002

I. INTRODUCTION

The slowing down of Moore's law has been driving the development of domain-specific computers in different fields. One approach is to build physics-inspired computers, exploiting the natural physics of materials and devices for efficiency. A prominent emerging example of "let physics do the computing" [1,2] is based on probabilistic bits (p-bits) [3–5]. The central idea in this field is to build *programmable* networks of p-bits, or p-circuits, the natural dynamic evolution of which leads to the solution of a problem of interest. The mathematical formulation of p-bits is related to the widely used Monte Carlo or

*Corresponding author: kemalselcuk@ucsb.edu
†Corresponding author: camsari@ucsb.edu

Markov chain Monte Carlo algorithms [6], casting a wide net for their application domains from random-number generation [7,8], machine learning [9,10], and combinatorial optimization [4,11] to a subset of quantum simulation problems [12–15].

Since their appearance as building blocks for probabilistic computation, there have been many proposals and implementations of p-bits in different material systems using a variety of stochastic phenomena [16–20]. A particularly promising possibility is the use of magnetic devices in the superparamagnetic regime; these have recently been shown to produce approximately gigahertz fluctuations at room temperature [21–24] using in-plane magnetic tunnel junctions (MTJs). Combined with the proven manufacturability of magnetic memory that has integrated billions of *deterministic* MTJs with standard complementary metal oxide semiconductor (CMOS) technology [25,26], the development of highly integrated and fast probabilistic computers is highly probable.

Despite successful recent demonstrations of fast superparamagnetism in in-plane MTJs, following earlier work on perpendicular MTJs [27,28], ideal stochastic MTJs (SMTJs) for *circuit-level* p-bits have been difficult to realize. In particular, a three-transistor–one-MTJ design (3T-1MTJ) [29] has been explored as a compact and energy-efficient implementation of a p-bit in discrete [4,9,14,30] and integrated implementations [31]. Various other possibilities beyond the 3T-1MTJ p-bit design have been considered, including a spin-orbit-torque design (proposed in Ref. [3]) and later experimentally demonstrated in Ref. [32] and by a comparator-based design [14,30], with possibly different SMTJ requirements. Moreover, entirely different approaches to create p-bits exploiting the stochasticity observed in the switching characteristics of *deterministic* MTJs have been proposed [33–37]. Here, we focus on the necessary design requirements for the 3T-1MTJ p-bit. This design makes minimal modifications to the currently integrated 1T-1MTJ circuit in commercialized spin-transfer-torque magnetoresistive random-access memory. The 3T-1MTJ p-bit does not explicitly require spin-torque control on magnetization characteristics, and its variation tolerance is greatly improved since it uses low-barrier nanomagnets.

There are several requirements for scalable SMTJ-based p-bits in this 3T-1MTJ p-bit circuit. First, the SMTJ design should be magnetically soft, fluctuating without requiring external magnetic fields, but electronically hard so that, even at large bias currents, the free-layer magnetization is not pinned. Second, the SMTJs should exhibit reasonable tunneling magnetoresistance (TMR), with *uniform* randomness in resistance values [38]. Third, the SMTJ should exhibit *fast* fluctuations. A previous design [39] using double free layers nearly satisfies all these requirements by providing fast zero-field fluctuations and bias independence (Fig. 1). The simplicity of the double-free-layer structure is appealing, as opposed to asymmetrically designed typical MTJs with fixed and free layers. However, achieving zero-bias and zero-field fluctuations comes at a price: for the thermal noise to overcome dipolar coupling between free layers, the magnetic layers need to be scaled down to about 20 nm or below, imposing fabrication challenges.

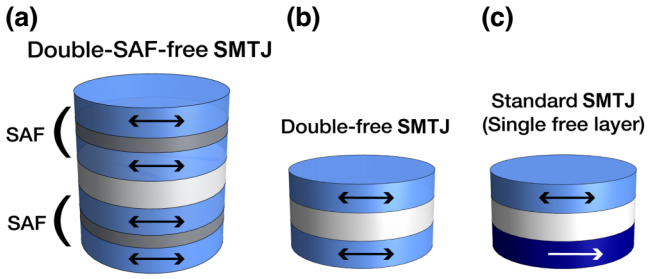

FIG. 1. SMTJ designs. (a) This work, double-SAF-free SMTJ, where the low-barrier free layers are replaced by magnetically inert SAF layers. (b) Double-free-layer SMTJ, with no fixed layer but two low-barrier free layers. (c) Standard SMTJ with a fixed layer and a low-barrier free layer; commonly used in the literature, since it minimally modifies existing stable MTJs with a fixed layer to have a low-barrier free layer.

Here, we propose an improvement to this earlier design by considering double-free-layer SMTJs using *synthetic antiferromagnetic* (SAF) free layers (Fig. 1). The key is to use the magnetic neutrality of SAF layers. Because the SAF layers possess antiparallel nanomagnets in close proximity, the net dipolar field emanating from the SAF layers is minimal, unlike single nanomagnets, the dipolar fields of which favor an antiparallel configuration of the two free layers, as in the case of double-free-layer SMTJs [39].

In the rest of this paper, we evaluate this proposed design through the language of spin circuits, as pioneered by Brataas *et al.* [40]. Furthermore, we employ coupled stochastic Landau-Lifshitz-Gilbert (SLLG) equations to take magnetization dynamics into account. We apply a microscopic approach to calculate the dipolar tensors between magnets and provide an approximate autocorrelation theory with analytical results. We then simulate the proposed SMTJ in conjunction with advanced transistor nodes in SPICE, estimating energy and delays to produce random bits.

II. SPIN-CIRCUIT AND STOCHASTIC LLG ANALYSIS OF THE PROPOSED SMTJ

Our approach here is to start from the powerful spin-circuit approach, as pioneered by Brataas *et al.* [40], that is converted into explicit circuit models, which can be modularly simulated in SPICE-like simulators [41–43]. These two approaches have been extensively compared and found to be exactly equivalent [43,44]. The

advantage of writing down explicit SPICE-compatible 4×4 conductances is the ability to combine spin, the transport physics obtained from the spin-circuit approach with time-dependent stochastic LLG solvers, and advanced CMOS transistor models, all in standard circuit simulators. The SLLG solvers are rigorously benchmarked against probabilistic models, such as the Fokker-Planck equation applied to nanomagnet dynamics [45,46]. This approach allows us to consider each interface separately, and it can be used to provide a detailed understanding of spin currents as they travel through the four-magnet system. Technically, the use of spin-circuit theory is strictly applicable to *metallic* interfaces [40] and modeling *tunneling* junctions requires a different treatment, such as multiplying the conductance matrices [47] to get a tunneling magnetoresistance ratio of $2P^2/(1-P^2)$, rather than the giant magnetoresistance ratio of $P^2/(1-P^2)$, where P is the interface polarization. Nevertheless, to keep our model fine-grained and microscopic at each interface, we use the metallic spin-circuit models (as in Ref. [48]) to study the proposed double-SAF-free MTJs as a series of ferromagnet–normal-metal interfaces. To match experiments, we choose the interface polarizations (P) appropriately, corresponding to experimental TMR values (shown in Table I).

Figure 2 shows how we decompose the full double-SAF-free layers into corresponding interfaces. F | N denotes a ferromagnet–normal-metal interface; NM denotes a normal nonmagnetic metal. All spin circuits are described by four-component currents (3 for spin and 1 for charge) related to 4×4 conductance matrices [Fig. 2(a)]. For the spacer in the SAF layers, we explicitly consider the NM layers (modeling ruthenium), but we do not include an explicit NM layer between the free layers for MgO. In our full model (Fig. 2) coupling transport and magnetism, we parameterize the F | N interfaces with instantaneous magnetization vectors obtained from the SLLG equations. We assume that the transport timescales are much faster than magnetization dynamics; hence, we assume a lumped circuit model for each magnetization vector [45]. The details of the 4×4 conductance models and the SLLG solver we use here have been explained in detail in Refs. [43–45].

III. EQUILIBRIUM (ZERO-BIAS) BEHAVIOR

In this section, we study the zero-bias behavior of the double-SAF-free-layer SMTJs under the influence of thermal noise and dipolar and interlayer-exchange interaction fields. We first describe the magnetostatics model we use here. We consider four identical magnets with the same volume, interacting with dipolar and exchange interactions. The magnets are assumed to be perfectly circular and zero barrier ($k_B T \ll 1$) with easy-plane anisotropy in the x-y plane. In Sec. V, we carefully analyze the validity of the easy-plane assumption. The equilibrium-energy description for this system is [50]

$$E = -2\pi M_s^2 \text{Vol.} \left(\sum_{i=1}^{n=4} \hat{m}_i^{\mathrm{T}} N_{ii} \hat{m}_i + \sum_{\substack{i,j \\ i \neq j}}^{n=4} \hat{m}_i^{\mathrm{T}} (J_{ij} + D_{ij}) \hat{m}_j \right), \tag{1}$$

where M_s represents the saturation magnetization; Vol. is the volume of each magnet; $\hat{m}_i$ are the three-dimensional magnetization vectors on the unit sphere; and N_{ii}, D_{ij}, and J_{ij} are the demagnetization, dipolar, and exchange tensors, respectively. We only consider exchange interactions between SAF pairs (1,2) and (3,4), while dipolar interactions are considered between all $\binom{4}{2} = 6$ pairs of magnets. Throughout this paper, we assume $N_{zz} = -1$ for all magnets, with all other components of the demagnetization tensor being zero. Note that this is a simplifying assumption and corrections to the demagnetization tensor [51] should be considered, depending on magnet geometry, for more detailed models.

In Eq. (1), we assume an isotropic and constant-exchange model, where the exchange tensor, J_{ij}, is parameterized by a single number, i.e., $J_{ij} = J_0 \delta_{ij}$. We renormalize the exchange coupling, J_{ex}, typically measured in units of J/m^2 [52], such that $J_0 = J_{\text{ex}}/(2\pi M_s^2 t)$, where t is the thickness of the magnets (assumed to be equal). In this form, J_{ij} has the same units as dipolar tensors and can be directly compared. Throughout, we use a $|J_{\text{ex}}|$ value of 5 mJ/m^2 for our numerical models, a reasonable choice considering experimental measurements [52,53]. To calculate dipolar tensors, D_{ij}, we follow the approach described in Ref. [39]. The basic idea is to obtain position-dependent dipolar tensors, $D_{ij}(x,y,z)$, starting from the Poisson equation for the magnetic potential, Ψ, $\nabla^2 \Psi = \nabla \cdot \hat{m}$, to calculate dipolar tensors, and then to *average* these tensors over the volume of the target magnet to obtain single D_{ij} values. Until the averaging step, this approach is exact. Due to the cylindrical symmetries present, the only nonzero components are $D_{xx} = D_{yy} = -D_{zz}/2$, where (x,y) are the easy-plane components and z is the out-of-plane component. In the rest of the paper, we drop the coordinate subscripts and use D for $D_{xx} = D_{yy}$.

To study the equilibrium behavior of this system, we perform numerical and theoretical analysis. For our numerical results, after calculating all six D values for each pair of magnets and assuming a fixed interlayer-exchange coupling between the SAF layers, we employ our full model in Fig. 2 with four coupled SLLGs to obtain the average $\cos\theta$ between layers 2 and 3, which determines the output signal. The dipolar coefficients and the numerical average of $\cos\theta$ are shown in Figs. 3(a) and 3(b), respectively. We study the average angle as a function of changing magnet thickness, t. Using a revised model

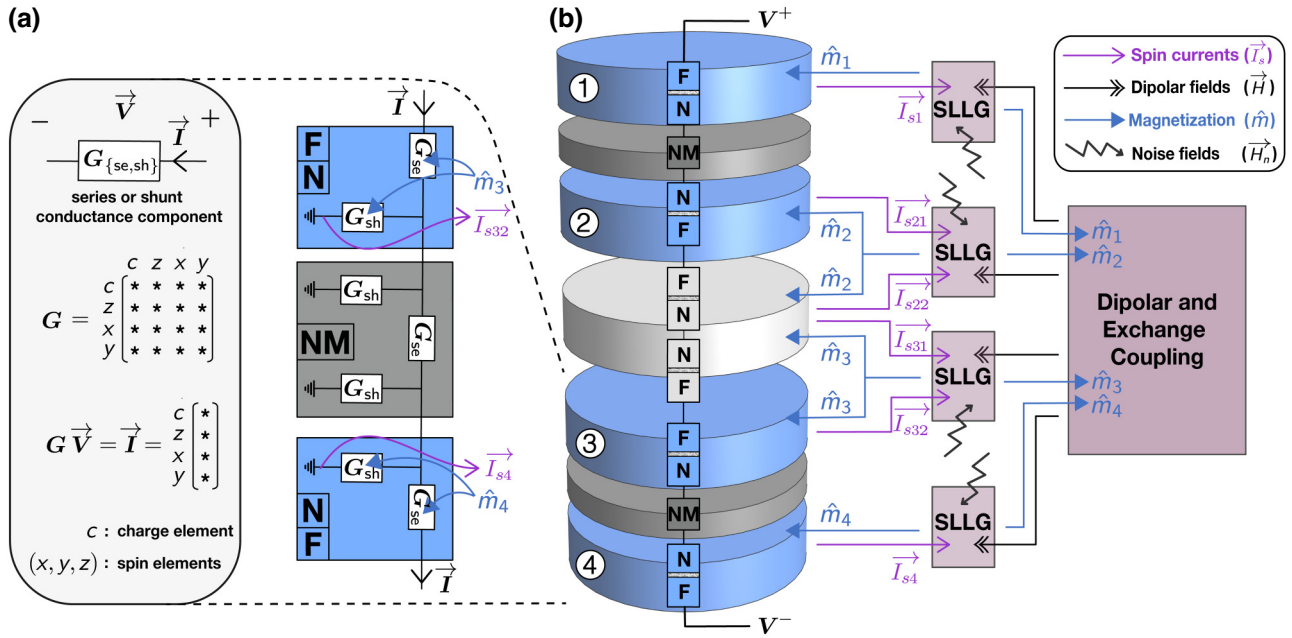

FIG. 2. Modular spin-circuit model for the double-SAF-free-layer structure. (a) Close-up look on the spin-circuit transport model for a single SAF stack layer; represented with two ferromagnet-normal metal (F | N) interfaces and a normal-metal (NM) block. (b) Full model coupling magnetization dynamics (SLLG) with spin-transport modules. Transport module produces spin-polarized currents as inputs to SLLGs. For the two interfaces of the same magnet, we add the spin currents incident to the magnets vectorially (e.g., $\vec{I}_{s2} = \vec{I}_{s21} + \vec{I}_{s22}$) as inputs to the SLLGs, since we are in the monodomain approximation for the magnets. LLGs, in turn, produce instantaneous magnetization vectors back to the interface modules. In addition, the two interfaces of the same magnet receive the same magnetization vector from their corresponding SLLGs as shown. Dipolar, exchange, and thermal noise are considered by the SLLG model. Details of the 4 × 4 conductances and the SLLG module can be found in Refs. [43–45,49]. Numerical parameters are summarized in Table I.

without the use of SAF free layers, but two FM | NM layers in series, we also closely reproduce the results from Ref. [39]. Ideally, $\langle \cos\theta \rangle$ should be zero, corresponding to freely fluctuating and truly independent stochastic free layers. As shown by the gray triangles in Fig. 3(b), for the double-free SMTJ (without the use of SAFs), reaching such an independent regime requires extremely thin magnets at small diameters (< 20 nm). The proposed MTJ with double SAF layers, on the other hand, shows near independence, even at large diameters, for a range of ferromagnet thicknesses, indicating the magnetic inertness of the SAF layers.

Next, we provide an approximate theoretical analysis for the results shown in Fig. 3. To proceed, we make simplifying assumptions. First, unlike our numerical model, which assumes a finite exchange coupling, for our theoretical calculation, we assume an effectively infinite exchange coupling between layers (1,2) and (3,4), which share a ruthenium spacer between them. We note that this is simply a mathematical infinity; in practice, using experimentally achievable exchange coupling coefficients justifies this assumption. This allows us to simplify the energy equation by substituting $m_1^{x,y,z}$ with $-m_2^{x,y,z}$ and $m_4^{x,y,z}$ with $-m_3^{x,y,z}$ and removing constant terms from the energy, as they do not change the Boltzmann probabilities:

$$E = -2\pi M_s^2 \mathrm{Vol.} \left(D_{23}\hat{m}_2^{\mathrm{T}}\hat{m}_3 - D_{13}\hat{m}_2^{\mathrm{T}}\hat{m}_3 - D_{24}\hat{m}_2^{\mathrm{T}}\hat{m}_3 + D_{14}\hat{m}_2^{\mathrm{T}}\hat{m}_3\right), \tag{2}$$

allowing us to obtain an "effective" dipolar tensor between layers 2 and 3:

$$E = -2\pi M_s^2 \mathrm{Vol.} \left[(D_{\mathrm{eff}})\hat{m}_2^{\mathrm{T}}\hat{m}_3\right], \tag{3}$$

where $D_{\mathrm{eff}} = D_{23} - D_{13} - D_{24} + D_{14}$. Figure 3(a) shows D_{eff} for magnets with $t = 1$ nm at varying diameters, Φ. We observe an approximate $D_{\mathrm{eff}} \propto \Phi^{-2}$ dependence, with a decreasing effective dipolar coupling at larger diameters. These results indicate how the double SAF layer reduces the effective coupling between layers 2 and 3. Next, we use the theoretical calculation presented in Ref. [39], where the equilibrium $\langle \cos\theta \rangle$ is related to the dipolar coupling coefficient, D, between two magnets. The idea behind this calculation is to assume a large demagnetization field and expand the Boltzmann probability, $\rho = 1/Z \exp(-E/k_{\mathrm{B}}T)$, around the out-of-plane component,

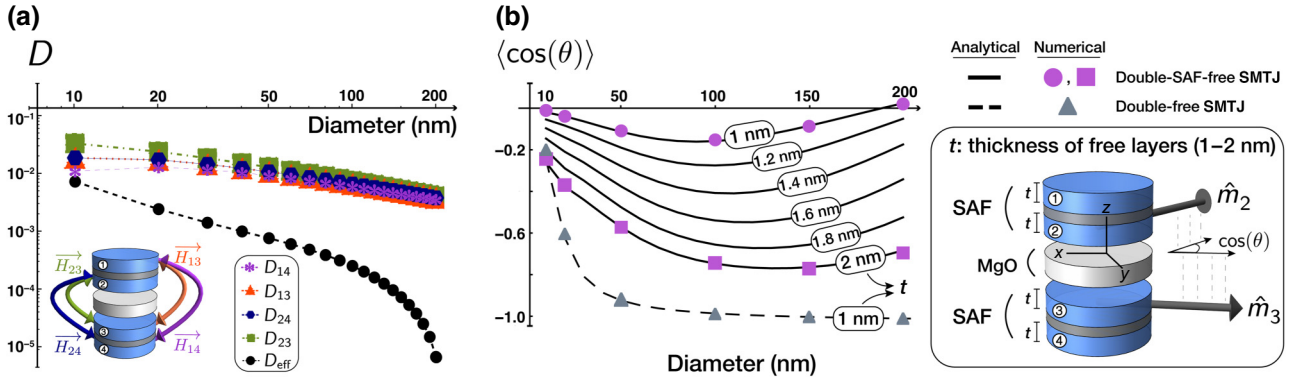

FIG. 3. Dipolar coupling in the double-SAF-free-layer structure (a) Dipolar coupling coefficients, D_{ij}, between magnets (i,j) are shown at varying diameters (1 nm thickness), numerically calculated based on the approach described in Ref. [39]. Effective dipolar (D_{eff}) coupling [Eq. (3)] is also shown. D_{12} and D_{34} are combined with exchange tensor (J_{ij}) for SAF couples in the numerical model but are not shown in the plot. (b) Average angles between layers (2,3), $\langle \cos\theta \rangle$, are calculated numerically (markers) and analytically (solid and dashed lines), based on [Eq. (4)], as a function of varying magnet diameters and thicknesses. Numerical calculations for the SLLG model uses a 1-ps time step and averages are taken over 5 μs.

since $m_z \approx 0$ for an analytical approximation. Note that, for this analysis, we do not set m_z to 0, but retain the first-order terms. With this approach, one obtains (in mks units)

$$\langle \cos\theta_{2,3} \rangle \approx \frac{I_1(d_{\text{eff}})}{I_0(d_{\text{eff}})}, \tag{4}$$

where I_n represents the modified Bessel function of the first kind and $d_{\text{eff}} = h_d D_{\text{eff}}$, where $h_d = \mu_0 M_s^2 \text{Vol.}/k_B T$ and μ_0 is the permeability. Using the D_{eff} values obtained at different diameters with Eq. (4), we obtain excellent agreement between theory and our numerical model, which does not assume an infinite exchange coupling between layers (1,2) and (3,4), as shown in Fig. 3(b). We note that the reason for the roughly constant and small $\cos(\theta) \approx 0 - 0.1$ at small thickness ($t = 1$ nm) can be explained by the cancellation of the approximate inverse square-law dependence of the dipolar coefficient on the diameter and the square-law dependence of the dipolar energy (in h_d) on the diameter. The results shown in Fig. 3 indicate that, to overcome the dipolar energy between layers (2,3), using a small volume and small-thickness magnets are still favorable, as in double-free-layer SMTJs [39]. Making Co-Fe-B-type magnets too thin (below < 2 nm) may induce perpendicular anisotropy in circular magnets [54], possibly necessitating further experimental optimization or different material systems.

IV. AUTOCORRELATION THEORY

Next, we provide an autocorrelation theory for the relative angle between magnetic layers (2,3), and compare it against our full numerical model (Fig. 2). We are interested in computing the quantity

$$C[\cos\theta(\tau)] = \frac{1}{T}\int_0^T \cos\theta(t+\tau)\cos\theta(t)dt, \tag{5}$$

where $\cos\theta$ represents the angle between layers (2,3). To simplify our analysis, to first order, we assume that the magnets always remain in the x-y plane and assume $m_z(t) \approx 0$, making $\cos\theta(t) = m_2^x(t)m_3^x(t) + m_2^y(t)m_y^3(t)$. Technically, the (x,y) components of magnets (2,3) are always correlated, as established in Fig. 3; however, at low thicknesses, they are only *weakly* correlated. As such, for our theoretical analysis, we make another simplifying assumption and assume that the magnets are independent of each other. This essentially means that we only need an analytical approximation for the autocorrelation of the m_x and m_y components. Following the analysis shown in Refs. [55,56], we proceed as follows. In circular nanomagnets, the mechanism of random fluctuations arises from the random precession of the in-plane magnetization vector around the stochastically fluctuating demagnetization field, which is a function of the out-of-plane component. The autocorrelation of the in-plane magnetization vector, $m_x(t)$, can be written as $C[m_x(\tau)] = \langle m_x(\tau)m_x(0)\rangle$, which is

$$\int_{-\infty}^{\infty} \cos(\alpha m_z)\exp(-\beta m_z^2)\,dm_z \Big/ \int_{-\infty}^{\infty} \exp(-\beta m_z^2)\,dm_z, \tag{6}$$

where α and β are defined as $\gamma H_d \tau$ and $H_d M_s \text{Vol.}/2k_B T$, respectively, while H_d is the out-of-plane demagnetization field and γ is the gyromagnetic ratio. The integral limits are extended to infinity to obtain a closed-form expression with minimal errors, due to the exponentially low probability of large m_z components. This expression is evaluated

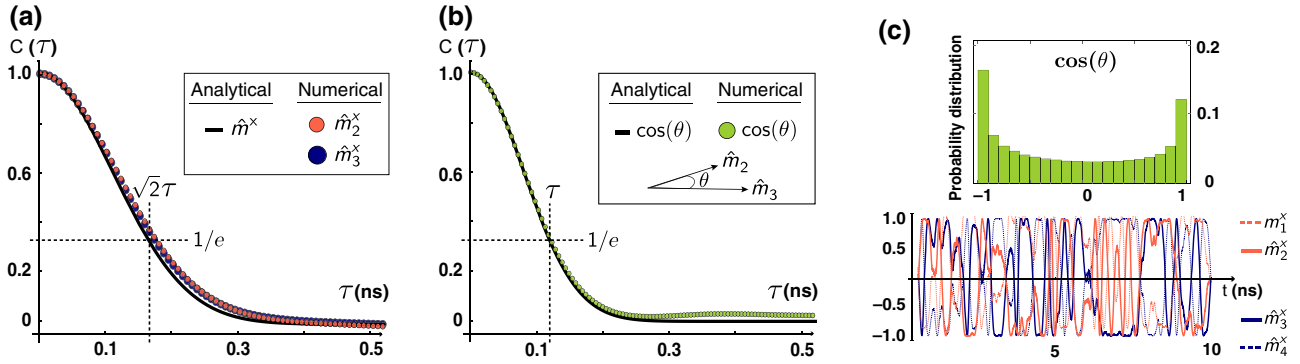

FIG. 4. Autocorrelation of magnetization. (a) Numerical and theoretical autocorrelation for the in-plane component of layers (2,3). (b) Numerical and theoretical autocorrelation of $\cos\theta$. Numerical results are obtained for a diameter of 50 nm and thickness $t = 1$ nm. Numerical results are obtained over 5 μs using a time step of 1 ps in SLLG simulations. (c) Time-dependent magnetizations of all layers from the full numerical model. Histogram for the cosine of the angle between layers $(2, 3)$ $\cos\theta$, demonstrating the necessary near-uniform randomness between -1 and $+1$ for p-bit operation.

as

$$C[m_x(\tau)] = \exp\left(-\frac{\alpha^2}{2\beta}\right). \tag{7}$$

In the present context, however, we are interested in the cosine of the angle between layers 2 and 3. As such, the autocorrelation expression (assuming both magnets remain in their x-y plane) becomes

$$\frac{\iint_{-\infty}^{+\infty} \cos[\alpha(m_{z1} - m_{z2})] \exp[-\beta(m_{z1}^2 + m_{z2}^2)] d\mathbf{m}_z}{\iint_{-\infty}^{+\infty} \exp[-\beta(m_{z1}^2 + m_{z2}^2)] d\mathbf{m}_z}, \tag{8}$$

which can be evaluated as

$$C[\cos(\theta(\tau))] = \exp\left(-\frac{\alpha^2}{\beta}\right). \tag{9}$$

We observe an interesting difference between previously obtained Eq. (7) [56] and Eq. (9). It turns out that the autocorrelation of the angle between the two independent magnets decays to $\exp(-1)$ of its value $\sqrt{2}$ times as fast as the autocorrelation of a single magnet. We corroborate this theoretical calculation with our full numerical model without any independence or in-plane rotation assumptions. We observe that, at moderate diameters of 50 nm with thicknesses of 1 nm, the SAF layers behave as if they were nearly independent of one another. The theoretically obtained $\sqrt{2}$ factor is also observed from our numerical simulations in Fig. 4. Faster decays of the autocorrelation on $\cos\theta$ bode well for probabilistic computing applications, since they directly influence the speed with which new and independent random numbers can be obtained from SMTJ-based p-bits.

V. OUT-OF-PLANE MAGNETIZATION BEHAVIOR

Our numerical results have been obtained using the simulation parameters shown in Table I, without making any assumptions about the out-of-plane magnetization components. Our analytical results, however, both for Eq. (4) and for Eq. (9), rely on the out-of-plane magnetization components being small. Here, we analyze the validity of this assumption both theoretically and numerically. First, considering a single easy-plane circular nanomagnet, the energy of which is

$$E = H_D M_s \text{Vol.}(m_z^2)/2, \tag{10}$$

where H_D is the demagnetization field. From the Boltzmann law, we can compute the variance of the out-of-plane component, $\langle m_z^2\rangle = \langle\cos^2(\theta)\rangle$, from

$$\langle m_z^2\rangle = \frac{1}{Z}\int_{\phi=0}^{\phi=2\pi}\int_{\theta=0}^{\theta=\pi} d\theta d\phi \cos^2(\theta)\sin(\theta)\exp(-E/k_B T), \tag{11}$$

which is evaluated as

$$\langle m_z^2\rangle = \frac{1}{h_d} - \frac{\exp(-h_d/2)}{\sqrt{\pi h_d/2}\,\text{erf}\left(\sqrt{h_d/2}\right)} \quad \text{(IMA)}, \tag{12}$$

where $h_d = H_D M_s \text{Vol.}/k_B T$ and IMA is in-plane magnetic anisotropy. Figure 5 compares Eq. (12) with numerical solutions of LLG as a function of magnet diameter with excellent agreement. Interestingly, in the case of SAFs where two nanomagnets are exchange coupled, the fluctuations (m_z^2) for out-of-plane components of each magnet are *reduced* by a factor of 2. This can be understood analytically by considering the energy of two exchange-coupled

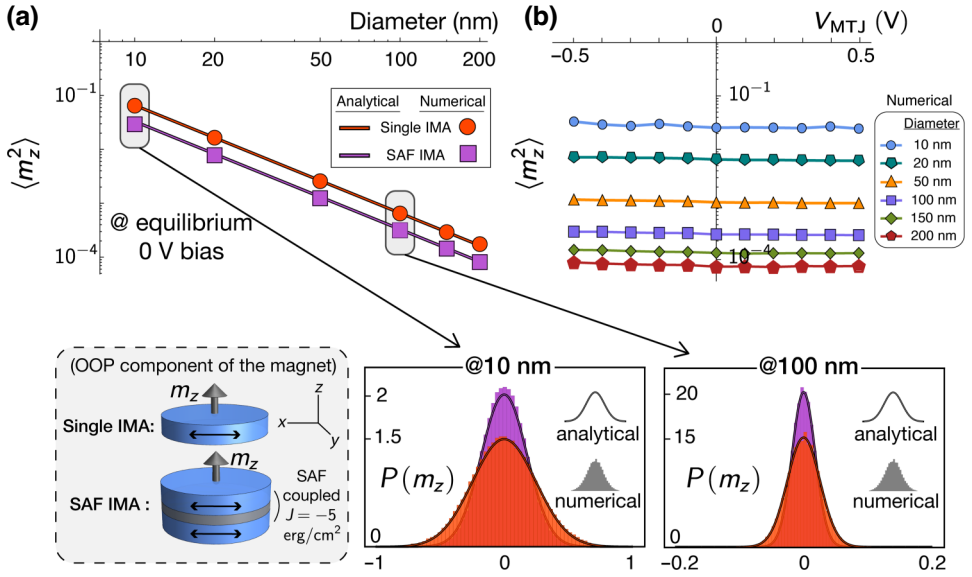

FIG. 5. Out-of-plane (OOP) magnetizations of easy-plane SAFs and single nanomagnets. (a) Out-of-plane components of magnets m_z^2 are evaluated as a function of diameter analytically [Eqs. (12)–(15)] and numerically for single and SAF easy-plane magnets at zero bias (equilibrium), along with their probability distributions obtained from the Boltzmann law [$\rho \propto \exp(-E)$]. (b) $\langle m_z^2 \rangle$ is shown numerically at different voltage biases from −0.5 to 0.5 V for a range of diameters from 10 to 200 nm with a free-layer thickness of 1 nm. Each point is averaged over 250-ns simulations with 1-ps transient time steps using the .trannoise function in HSPICE.

easy-plane nanomagnets:

$$E = \text{Vol.}\left[H_D M_s \sum_{i\in\{1,2\}} \frac{\cos^2\theta_i}{2} - 2J_{\text{ex}}(\hat{m}_1 \cdot \hat{m}_2)\right], \quad (13)$$

where $\cos\theta_i$ is the out-of-plane component of each easy-plane magnet. For the experimentally relevant exchange-coupling values, $J_{\text{ex}} \approx -5$ erg/cm^2, we find that the exchange interaction dominates the demagnetization and thermal fields. In such a scenario, we are justified to assume $\hat{m}_1 \cdot \hat{m}_2 \approx -1$ in the general energy equation [Eq. (13)] using the parity transformation ($\theta_2 \to \pi - \theta_1$ and $\phi_1 \to \pi + \phi_2$), leading to

$$E = \left(\frac{h_d}{2} + j_{\text{ex}} + \frac{h_d}{2}\cos 2\theta_1\right), \quad (14)$$

where j_{ex} is reduced to a dimensionless value similar to h_d. Following a similar prescription to that in Eq. (11) to compute the average out-of-plane fluctuations for SAF magnets, we get

$$\langle m_z^2 \rangle = \frac{1}{2h_d} - \frac{\exp(-h_d)}{\sqrt{\pi h_d}\,\text{erf}\left(\sqrt{h_d}\right)} \quad \text{(SAF)}. \quad (15)$$

Comparing Eq. (15) with Eq. (12), we observe that the strong SAF coupling effectively doubles the demagnetization field and reduces fluctuations. Figure 5 shows that the numerical behavior is well explained by Eq. (15). In our present context, the use of SAFs as free layers, compared to single easy-plane magnets [39], favorably decreases out-of-plane fluctuations, making our assumptions more reliable. Below < 20 nm however, one must be careful with these assumptions, since large out-of-plane fluctuations may be observed. Finally, Fig. 5(b) shows the fluctuations under voltage bias conditions, the details of which are discussed in Sec. VI. We observe that the large demagnetization fields present, along with the antisymmetric magnetic configuration, do not lead to instabilities (at least in the parameter ranges of interest we consider here), exhibiting bias independence for the out-of-plane fluctuations. These results are in line with earlier work, where easy-plane magnets exhibit large pinning fields [55].

VI. NONEQUILIBRIUM (BIAS-DEPENDENT) BEHAVIOR

We now investigate the bias dependence of our proposed device, using the full numerical model of Fig. 2. Considering self-consistent finite-temperature magnetization, dipolar exchange fields, and spin circuits for transport, we numerically measure $\cos\theta$ at different bias voltages, as shown in Figs. 6(a) and 6(b). We choose experimentally informed conductance and polarization parameters for the MTJ and ruthenium interfaces, as shown in Table I. Even though we treat the SAF layers as spin valves composed of

TABLE I. Simulation parameters.

Parameter	Value
Co-Fe-B/MgO/Co-Fe-B RA product	$9\,\Omega\,\mu m^2$ [57]
Co-Fe-B/Ru/Co-Fe-B RA product	$5.2 \times 10^{-3}\,\Omega\,\mu m^2$ [58] [59]
↳ corresponding G_0	(1/RA product)/area $\mho$
Temperature	300 K
M_s	8×10^5 A/m [39]
Damping coefficient (α)	0.01 [60]
Real part of g_{mix}, ($G_0 a$)	$a = 1$ [44,61]
Imaginary part of g_{mix}, ($G_0 b$)	$b = 0$ [44]
λ_{sf} of Ru layer	14 nm [62]
P_0 of Co-Fe-B/MgO/Co-Fe-B, TMR	0.73, TMR = 115% [39]
P_0 of Co-Fe-B/Ru/Co-Fe-B, GMR	0.077, GMR = 0.6% [63]
Diameters of SMTJs, used in p-bit	{10, . . . , 200} nm, 25 nm
Aspect ratio of free layer	1
Thickness of free layer, Ru layer	1–2 nm, 0.8 nm [54]
Exchange field (J_{ex})	-5×10^{-3} J/m^2 [52]
CMOS models	14 nm HP-FinFET [64]

F|N interfaces, due to their relatively small interface polarizations, the main resistance modulation arises between layers 2 and 3, which are separated by the MgO layer.

To test our fine-grained spin-circuit model, which splits the system into individual F|N interfaces, we first design a spin-valve structure with two F | N interfaces to study the double-free-layer SMTJ proposed in Ref. [39]. Without any assumptions for the spin currents, we observed the same bias independence using our spin-circuit model with quantitatively similar results to those in Ref. [39], which used a phenomenological model with explicitly defined antisymmetric spin currents [Fig. 6(b)]. This indicates that our fine-grained interface model captures detailed physics accurately. We observe that the double-free-layer SMTJ shows significant correlations, measured by $\cos\theta$ for diameters above 50 nm, where the magnets are completely pinned in antiparallel directions.

Next, we use our full numerical model to investigate the bias dependence of $\cos\theta$ for the double-SAF-layer structure [Fig. 6(a)]. We observe that, for a large range of diameters, $\cos\theta$ shows a weak bias dependence and is close to zero. In addition, the double-SAF-free SMTJ should be robust against external magnetic fields, due to the magnetic insensitivity of the SAF layers [54]. We believe that our proposed design is a promising stochastic MTJ, since it satisfies the three important conditions of (a) bias independence [Fig. 6(a)]; (b) uniform randomness in the relative magnetization angle [Fig. 4(c)]; and (c) fast fluctuations, without requiring external magnetic fields [Fig. 4(b)]. Our design improved upon earlier ones, where the dipolar interaction between two closely separated nanomagnets was either ignored entirely [29] or required single-digit magnet diameters [39] with challenging fabrication requirements. Given the recent experimental success in observing

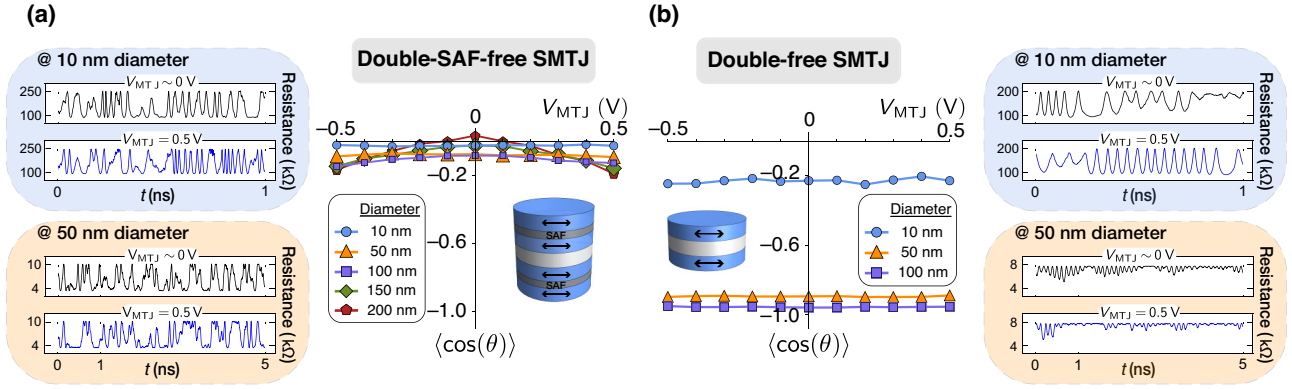

FIG. 6. Bias dependence of SMTJs. (a) Time-averaged $\cos\theta$ as a function of bias voltage across the MTJs for the double-SAF-free SMTJ. Left-hand side shows corresponding resistance fluctuations at chosen diameters of 10–50 nm and bias points of 1 mV–0.5 V. Fluctuation rates are inversely proportional to device diameter, Φ, as predicted by Eq. (9). Device exhibits independence between the free layers, $\langle\cos\theta\rangle \approx 0$, with bias independence. (b) Time-averaged $\cos\theta$ as a function of bias voltage for a double-free SMTJ, modeled as two F | N interfaces in series. Right-hand side shows corresponding resistance fluctuations at chosen diameters of 10–50 nm and bias points of 1 mV–0.5 V. These results are in quantitative agreement with the phenomenological model introduced in Ref. [39]. Unlike that model, however, we do not legislate antisymmetric currents to the magnets at the interfaces. This behavior comes out of our fine-grained interface model. Moreover, due to the uncompensated for dipolar coupling, the double-free SMTJ does not exhibit nearly independent fluctuations between its layers, $\langle\cos\theta\rangle \neq 0$. All magnets are assumed to have a thickness of 1 nm. Each data point is averaged over 1 μs, with a time step of 1 ps using the .trannoise function in HSPICE.

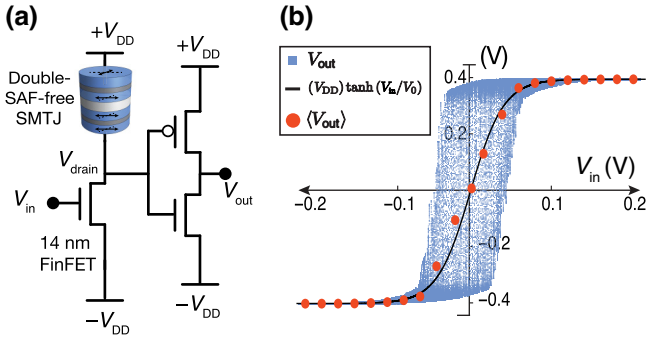

FIG. 7. 3T-1MTJ p-bit circuit with double-SAF-free MTJ. (a) We use the full circuit model described in Fig. 2 in conjunction with a 14-nm HP-FinFET predictive model [65], simulated in HSPICE. Magnet diameters are 25 nm and thicknesses are 1 nm. Diameter is chosen to match transistor resistance. (b) Blue trace is observed by observing V_{out} as a function of V_{in}, while V_{in} is linearly swept from -0.2 to 0.2 V in a 250-ns time window. Red dots are obtained as separate measurements, where V_{in} is fixed to a given value and a time average of the output over 5 μs is taken with a 1-ps time step. Black line is a tanh fit to this average.

nanosecond fluctuations in nanomagnets [21,22,24], the prospects for experimentally demonstrating the key features of double-SAF SMTJs seem promising. Indeed, a recent experiment employing SAF-based free- and fixed-layer stochastic MTJs (albeit with different thicknesses) [23] exhibits some of the key features of bias independence and nanosecond fluctuations.

VII. CMOS CIRCUIT BEHAVIOR AND PERFORMANCE

One of the main advantages of the self-consistent spin-circuit approach coupling microscopic transport physics with magnet dynamics in standard circuit simulators is in the ability to integrate them with existing CMOS models. Here, we combine our full device model presented in Fig. 2 with advanced predictive technology models for 14-nm FinFET (Fin field-effect transistor) transistors. Figure 7 shows the 3T-1MTJ topology [29] to design a p-bit with a binary output, the probability of which is controlled by an input voltage, V_{in}. The behavioral equation for the ideal p-bit is given by

$$m_i = \text{sgn}\left[\tanh\left(I_i\right) - \text{rand}_U\right]. \tag{16}$$

For this equation to produce a smoothly varying output probability and a mean of $\langle m\rangle = \tanh(I_i)$, an essential requirement is that the random noise denoted by rand_U is *uniform* and continuous between -1 and $+1$ [38]. To see how the 3T-1MTJ circuit maps to Eq. (16), we consider the time-varying drain voltage in Fig. 7(a) given by

$$\frac{V_{\text{drain}}}{2V_{\text{DD}}} = \frac{1}{2} - \frac{R_{\text{MTJ}}(t)}{R_{\text{MTJ}}(t) + R_{\text{DS}}(V_{\text{in}})}, \tag{17}$$

TABLE II. Performance measurements.

Power dissipation on SMTJ branch	6.6 μW
Power dissipation on inverter branch	5.3 μW
Flips per second	3.3 flips/ns
Energy per RNG (random number generation)	3.6 fJ

where $R_{\text{DS}}(V_{\text{in}})$ is the transistor resistance, which varies as a function of the input voltage. Equation (17) indicates another important design criterion for the 3T-1MTJ circuit to function as a p-bit, namely, for V_{drain} to produce equal 1 and -1 fluctuations at the output of the inverter, the *average* MTJ resistance needs to be matched to the transistor resistance when V_{in} is at the midpoint of the sigmoid (in our circuit, this is when $V_{\text{in}} = 0$). When biased in its midpoint ($V_{\text{drain}} = 0$), the main function of the inverter is to amplify V_{drain}, which can be approximated by a sign function, making the output

$$\frac{V_{\text{out}}}{V_{\text{DD}}} \sim \text{sgn}\left[R_{\text{DS}}\left(V_{\text{in}}\right) - R_{\text{MTJ}}(t)\right], \tag{18}$$

providing a circuit mapping to the behavioral Eq. (16). Figure 7 shows numerical results for this full circuit, indicating how the proposed double-SAF-free MTJ approximately produces the tunable randomness necessary for the p-bit. Next, using our SPICE model, we estimate several key metrics for p-bits. We delineate the power dissipation of the circuit into two branches, the SMTJ branch and the inverter branch. We obtain the power dissipation on the MTJ branch by measuring the instantaneous current flow over a 5-μs time window and multiplying this by the supply voltage, where the product is around 6.6 μW. Similarly, we measure the power dissipation on the inverter branch to be around 5.3 μW. We define a probabilistic flip based on the autocorrelation values from Fig. 4, where a new flip is defined as the time when the autocorrelation roughly saturates. We estimate such an independent flip time to be around $\tau_f = 0.3$ ns for the double-SAF-free MTJ. Using these numbers, the energy per random-number generation is estimated to be $P_{\text{total}} \times \tau_f \approx 3.6$ fJ. These values are reported in Table II, and they are in rough agreement with those estimated in Ref. [38]. The important point to note, however, is that the proposed SMTJ does not make any simplifying assumptions about dipolar fields, the necessary uniform randomness in the MTJ, or the speed of fluctuations. The total flips per second in a system of integrated p-bits, say with 10^6 p-bits fluctuating in sparsely connected networks, could lead to a system flips per second of $N/\tau_f = 3.3 \times 10^{15}$ sec^{-1}, which is 4–5 orders of magnitude larger than what can be achieved with present-day CMOS technology [11,66].

VIII. CONCLUSION

We proposed and analyzed a stochastic magnetic tunnel junction with double synthetic-antiferromagnetic free layers with a modular spin-circuit model. By theoretical analysis and numerical calculations, we have shown that the proposed stochastic MTJ can meet the important requirements of bias independence, uniform randomness, and fast fluctuations without any external magnetic fields. Similar to earlier double-free SMTJ designs, the structure should be relatively easy to build. The low-barrier nature of the constituent magnets should provide robustness against variations. Circuit analysis shows that the proposed device can function as a fast and energy-efficient p-bit design, which can aid in the development of large-scale probabilistic computers; this is useful for a wide variety of applications relevant to machine learning and artificial-intelligence algorithms.

ACKNOWLEDGMENTS

K.S. and K.Y.C. acknowledge support from the U.S. National Science Foundation (NSF) through CCF 2106260 and SAMSUNG Global Research Outreach (GRO) grants. Use was made of computational facilities purchased with funds from the National Science Foundation (CNS-1725797) and administered by the Center for Scientific Computing (CSC). The CSC is supported by the California NanoSystems Institute and the Materials Research Science and Engineering Center (MRSEC; NSF DMR 2308708) at UC Santa Barbara. S.F. and S.K. acknowledge support from JST-CREST JPMJCR19K3, JST-PRESTO JPMJPR21B2, JST-AdCORP JPMJKB2305, and JST-ASPIRE JPMJAP2322.

[1] R. P. Feynman, Simulating physics with computers, Int. J. Theor. Phys. **21**, 467 (1982).

[2] W. Porod, Quantum-dot devices and quantum-dot cellular automata, J. Franklin Inst. **334**, 1147 (1997).

[3] K. Y. Camsari, R. Faria, B. M. Sutton, and S. Datta, Stochastic p-bits for invertible logic, Phys. Rev. X **7**, 031014 (2017).

[4] W. A. Borders, A. Z. Pervaiz, S. Fukami, K. Y. Camsari, H. Ohno, and S. Datta, Integer factorization using stochastic magnetic tunnel junctions, Nature **573**, 390 (2019).

[5] S. Chowdhury, A. Grimaldi, N. A. Aadit, S. Niazi, M. Mohseni, S. Kanai, H. Ohno, S. Fukami, L. Theogarajan, G. Finocchio, S. Datta, and K. Y. Camsari, A full-stack view of probabilistic computing with p-bits: Devices, architectures, and algorithms, IEEE J. Explor. Solid-State Comput. Devices Circuits **9**, 1 (2023).

[6] D. Koller and N. Friedman, *Probabilistic Graphical Models: Principles and Techniques* (MIT Press, Cambridge, MA, 2009).

[7] D. Vodenicarevic, N. Locatelli, A. Mizrahi, J. S. Friedman, A. F. Vincent, M. Romera, A. Fukushima, K. Yakushiji, H. Kubota, S. Yuasa, S. Tiwari, J. Grollier, and D. Querlioz, Low-energy truly random number generation with superparamagnetic tunnel junctions for unconventional computing, Phys. Rev. Appl. **8**, 054045 (2017).

[8] P. Talatchian, M. W. Daniels, A. Madhavan, M. R. Pufall, E. Jué, W. H. Rippard, J. J. McClelland, and M. D. Stiles, Mutual control of stochastic switching for two electrically coupled superparamagnetic tunnel junctions, Phys. Rev. B **104**, 054427 (2021).

[9] J. Kaiser, W. A. Borders, K. Y. Camsari, S. Fukami, H. Ohno, and S. Datta, Hardware-aware *in situ* learning based on stochastic magnetic tunnel junctions, Phys. Rev. Appl. **17**, 014016 (2022).

[10] M. W. Daniels, A. Madhavan, P. Talatchian, A. Mizrahi, and M. D. Stiles, Energy-efficient stochastic computing with superparamagnetic tunnel junctions, Phys. Rev. Appl. **13**, 034016 (2020).

[11] N. A. Aadit, A. Grimaldi, M. Carpentieri, L. Theogarajan, J. M. Martinis, G. Finocchio, and K. Y. Camsari, Massively parallel probabilistic computing with sparse Ising machines, Nat. Electron. **5**, 460 (2022).

[12] K. Y. Camsari, S. Chowdhury, and S. Datta, Scalable emulation of sign-problem-free Hamiltonians with room-temperature p-bits, Phys. Rev. Appl. **12**, 034061 (2019).

[13] S. Chowdhury, K. Y. Camsari, and S. Datta, Emulating quantum circuits with generalized Ising machines, IEEE Access (2023).

[14] A. Grimaldi, K. Selcuk, N. A. Aadit, K. Kobayashi, Q. Cao, S. Chowdhury, G. Finocchio, S. Kanai, H. Ohno, S. Fukami, and K. Y. Camsari, in *2022 International Electron Devices Meeting (IEDM)* (IEEE, 2022), p. 22.4.1.

[15] S. Chowdhury, K. Y. Camsari, and S. Datta, Accelerated quantum Monte Carlo with probabilistic computers, Commun. Phys. **6**, 85 (2023).

[16] K. S. Woo, J. Kim, J. Han, W. Kim, Y. H. Jang, and C. S. Hwang, Probabilistic computing using $Cu_{0.1}Te_{0.9}/HfO_2/Pt$ diffusive memristors, Nat. Commun. **13**, 5762 (2022).

[17] Y. Liu, Q. Hu, Q. Wu, X. Liu, Y. Zhao, D. Zhang, Z. Han, J. Cheng, Q. Ding, Y. Han, B. Peng, H. Jiang, X. Xue, H. Lv, and J. Yang, Probabilistic circuit implementation based on p-bits using the intrinsic random property of RRAM and p-bit multiplexing strategy, Micromachines **13**, 924 (2022).

[18] T. J. Park, K. Selcuk, H. T. Zhang, S. Manna, R. Batra, Q. Wang, H. Yu, N. A. Aadit, S. K. R. S. Sankaranarayanan, H. Zhou, K. Y. Camsari, and S. Ramanathan, Efficient probabilistic computing with stochastic perovskite nickelates, Nano Lett. **22**, 8654 (2022).

[19] S. Deng, T. J. Park, H. Yu, A. Saha, A. N. M. N. Islam, Q. Wang, A. Sengupta, and S. Ramanathan, Hydrogenated VO_2 bits for probabilistic computing, IEEE Electron Device Lett. **44**, 1776 (2023).

[20] G. M. Gutiérrez-Finol, S. Giménez-Santamarina, Z. Hu, L. E. Rosaleny, S. Cardona-Serra, and A. Gaita-Ariño, Lanthanide molecular nanomagnets as probabilistic bits, npj Comput. Mater. **9**, 196 (2023).

[21] K. Hayakawa, S. Kanai, T. Funatsu, J. Igarashi, B. Jinnai, W. A. Borders, H. Ohno, and S. Fukami, Nanosecond random telegraph noise in in-plane magnetic tunnel junctions, Phys. Rev. Lett. **126**, 117202 (2021).

[22] C. Safranski, J. Kaiser, P. Trouilloud, P. Hashemi, G. Hu, and J. Z. Sun, Demonstration of nanosecond operation in stochastic magnetic tunnel junctions, Nano Lett. **21**, 2040 (2021).

[23] J. Z. Sun, C. Safranski, P. Trouilloud, C. D'Emic, P. Hashemi, and G. Hu, Easy-plane dominant stochastic magnetic tunnel junction with synthetic antiferromagnetic layers, Phys. Rev. B **108**, 064418 (2023).

[24] L. Schnitzspan, M. Kläui, and G. Jakob, Nanosecond true-random-number generation with superparamagnetic tunnel junctions: Identification of joule heating and spin-transfer-torque effects, Phys. Rev. Appl. **20**, 024002 (2023).

[25] S. Aggarwal, H. Almasi, M. DeHerrera, B. Hughes, S. Ikegawa, J. Janesky, H. K. Lee, H. Lu, F. B. Mancoff, K. Nagel, G. Shimon, J. J. Sun, T. Andre, and S. M. Alam, in *2019 IEEE International Electron Devices Meeting (IEDM)* (IEEE, 2019), pp. 2.1.1–2.1.4.

[26] K. Lee, *et al.*, in *2019 IEEE International Electron Devices Meeting (IEDM)* (IEEE, 2019), p. 2.2.1.

[27] B. Parks, M. Bapna, J. Igbokwe, H. Almasi, W. Wang, and S. A. Majetich, Superparamagnetic perpendicular magnetic tunnel junctions for true random number generators, AIP. Adv. **8**, 055903 (2018).

[28] T. Funatsu, S. Kanai, J. Ieda, S. Fukami, and H. Ohno, Local bifurcation with spin-transfer torque in superparamagnetic tunnel junctions, Nat. Commun. **13**, 4079 (2022).

[29] K. Y. Camsari, S. Salahuddin, and S. Datta, Implementing p-bits with embedded MTJ, IEEE Electron Device Lett. **38**, 1767 (2017).

[30] N. S. Singh, K. Kobayashi, Q. Cao, K. Selcuk, T. Hu, S.Niazi, N. A. Aadit, S. Kanai, H. Ohno, S. Fukami, and K. Y. Camsari, CMOS plus stochastic nanomagnets enabling heterogeneous computers for probabilistic inference and learning, Nat. Commun. **15**, 2685 (2024).

[31] J. Daniel, Z. Sun, X. Zhang, Y. Tan, N. Dilley, Z. Chen, and J. Appenzeller, Experimental demonstration of an integrated on-chip p-bit core utilizing stochastic magnetic tunnel junctions and 2D-MoS_2 FETs, arXiv:2308.10989.

[32] J. Yin, Y. Liu, B. Zhang, A. Du, T. Gao, X. Ma, Y. Dong, Y. Bai, S. Lu, Y. Zhuo, Y. Huang, W. Cai, D. Zhu, K. Shi, K. Cao, D. Zhang, L. Zeng, and W. Zhao, in *2022 International Electron Devices Meeting (IEDM)* (IEEE, 2022), p. 36.1.1.

[33] A. Fukushima, T. Seki, K. Yakushiji, H. Kubota, H. Imamura, S. Yuasa, and K. Ando, Spin dice: A scalable truly random number generator based on spintronics, Appl. Phys. Express **7**, 083001 (2014).

[34] L. Rehm, C. C. M. Capriata, S. Misra, J. D. Smith, M. Pinarbasi, B. G. Malm, and A. D. Kent, Stochastic magnetic actuated random transducer devices based on perpendicular magnetic tunnel junctions, Phys. Rev. Appl. **19**, 024035 (2023).

[35] Y. Shim, S. Chen, A. Sengupta, and K. Roy, Stochastic spin-orbit torque devices as elements for Bayesian inference, Sci. Rep. **7**, 14101 (2017).

[36] B. R. Zink, Y. Lv, and J.-P. Wang, Review of magnetic tunnel junctions for stochastic computing, IEEE J. Explor. Solid-State Comput. Devices Circuits **8**, 173 (2022).

[37] M. T. McCray, M. A. Abeed, and S. Bandyopadhyay, Electrically programmable probabilistic bit anti-correlator on a nanomagnetic platform, Sci. Rep. **10**, 12361 (2020).

[38] O. Hassan, S. Datta, and K. Y. Camsari, Quantitative evaluation of hardware binary stochastic neurons, Phys. Rev. Appl. **15**, 064046 (2021).

[39] K. Y. Camsari, M. M. Torunbalci, W. A. Borders, H. Ohno, and S. Fukami, Double-free-layer magnetic tunnel junctions for probabilistic bits, Phys. Rev. Appl. **15**, 044049 (2021).

[40] A. Brataas, G. E. W. Bauer, and P. J. Kelly, Non-collinear magnetoelectronics, Phys. Rep. **427**, 157 (2006).

[41] S. Srinivasan, V. Diep, B. Behin-Aein, A. Sarkar, and S. Datta, Modeling multi-magnet networks interacting via spin currents, arXiv:1304.0742.

[42] S. Manipatruni, D. E. Nikonov, and I. A. Young, Modeling and design of spintronic integrated circuits, IEEE Trans. Circuits Syst. I Regul. Pap. **59**, 2801 (2012).

[43] K. Y. Camsari, Ph.D. thesis, Purdue University, 2015.

[44] K. Y. Camsari, S. Ganguly, and S. Datta, Modular approach to spintronics, Sci. Rep. **5**, 10571 (2015).

[45] M. M. Torunbalci, P. Upadhyaya, S. A. Bhave, and K. Y. Camsari, Modular compact modeling of MTJ devices, IEEE Trans. Electron Devices **65**, 4628 (2018).

[46] S. Kanai, K. Hayakawa, H. Ohno, and S. Fukami, Theory of relaxation time of stochastic nanomagnets, Phys. Rev. B **103**, 094423 (2021).

[47] K. Y. Camsari, S. Ganguly, D. Datta, and S. Datta, in *2014 IEEE International Electron Devices Meeting* (IEEE, 2014), p. 35.6.

[48] S. Manipatruni, D. E. Nikonov, and I. A. Young, Vector spin modeling for magnetic tunnel junctions with voltage-dependent effects, J. Appl. Phys. **115**, 17B754 (2014).

[49] nanohub.org, Modular approach to spintronics, Available at: https://nanohub.org/groups/spintronics.

[50] I. D. Mayergoyz, G. Bertotti, and C. Serpico, *Nonlinear Magnetization Dynamics in Nanosystems* (Elsevier, 2009).

[51] M. Beleggia, M. De Graef, and Y. T. Millev, The equivalent ellipsoid of a magnetized body, J. Phys. D: Appl. Phys. **39**, 891 (2006).

[52] K. Yakushiji, H. Kubota, A. Fukushima, and S. Yuasa, Perpendicular magnetic tunnel junctions with strong antiferromagnetic interlayer exchange coupling at first oscillation peak, Appl. Phys. Express **8**, 083003 (2015).

[53] S. S. P. Parkin and D. Mauri, Spin engineering: Direct determination of the Ruderman-Kittel-Kasuya-Yosida far-field range function in ruthenium, Phys. Rev. B **44**, 7131 (1991).

[54] K. Kobayashi, K. Hayakawa, J. Igarashi, W. A. Borders, S. Kanai, H. Ohno, and S. Fukami, External-field-robust stochastic magnetic tunnel junctions using a free layer with synthetic antiferromagnetic coupling, Phys. Rev. Appl. **18**, 054085 (2022).

[55] O. Hassan, R. Faria, K. Y. Camsari, J. Z. Sun, and S. Datta, Low-barrier magnet design for efficient hardware binary stochastic neurons, IEEE Magn. Lett. **10**, 1 (2019).

[56] J. Kaiser, A. Rustagi, K. Y. Camsari, J. Z. Sun, S. Datta, and P. Upadhyaya, Subnanosecond fluctuations in low-barrier nanomagnets, Phys. Rev. Appl. **12**, 054056 (2019).

[57] C. J. Lin, S. H. Kang, Y. J. Wang, K. Lee, X. Zhu, W. C. Chen, X. Li, W. N. Hsu, Y. C. Kao, M. T. Liu, W. C.

Chen, Yi-Ching Lin, M. Nowak, N. Yu, and Luan Tran, in *2009 IEEE International Electron Devices Meeting (IEDM)* (IEEE, 2009), p. 1.

[58] A. K. Pal, S. Chaudhuri, and A. K. Barua, The electrical resistivity and temperature coefficient of resistivity of cobalt films, J. Phys. D: Appl. Phys. **9**, 2261 (1976).

[59] X. Zhang, H. Huang, R. Patlolla, W. Wang, F. W. Mont, J. Li, C.-K. Hu, E. G. Liniger, P. S. McLaughlin, C. Labelle, E. T. Ryan, D. Canaperi, T. Spooner, G. Bonilla, and D. Edelstein, in *2016 IEEE International Interconnect Technology Conference / Advanced Metallization Conference (IITC/AMC)* (2016), pp. 31–33.

[60] J. C. Sankey, Y. T. Cui, J. Z. Sun, J. C. Slonczewski, R. A. Buhrman, and D. C. Ralph, Measurement of the spin-transfer-torque vector in magnetic tunnel junctions, Nat. Phys. **4**, 67 (2008).

[61] M. Tokaç, S. A. Bunyaev, G. N. Kakazei, D. S. Schmool, D. Atkinson, and A. T. Hindmarch, Interfacial structure dependent spin mixing conductance in cobalt thin films, Phys. Rev. Lett. **115**, 056601 (2015).

[62] K. Eid, R. Fonck, M. AlHaj Darwish, W. P. Pratt Jr., and J. Bass, Current-perpendicular-to-plane-magnetoresistance properties of Ru and Co/Ru interfaces, J. Appl. Phys. **91**, 8102 (2002).

[63] G. Gubbiotti, S. Tacchi, G. Carlotti, G. Socino, F. Spizzo, Z. Zhao, P. Mani, and G. J. Mankey, Interlayer exchange coupling in Co/Ru/Co trilayers, J. Magn. Magn. Mater. **286**, 468 (2005).

[64] Predictive Technology Model (PTM), Available at: http://ptm.asu.edu/.

[65] W. Zhao and Y. Cao, Predictive technology model for nano-CMOS design exploration, ACM J. Emerg. Tech. Comput. Syst. **3**, 1-es (2007).

[66] J. Romero, M. Bisson, M. Fatica, and M. Bernaschi, High performance implementations of the 2D Ising model on GPUs, Comput. Phys. Commun. **256**, 107473 (2020).